

Fracture Behavior Investigation of a Typical Sandstone Under Mixed-Mode I/II Loading Using the Notched Deep Beam Bending Method

Y. Luo¹ · L. Ren¹  · L. Z. Xie^{1,2} · T. Ai¹ · B. He²

Received: 4 July 2016 / Accepted: 18 April 2017 / Published online: 26 April 2017
© Springer-Verlag Wien 2017

Abstract The brittle fracture behavior of rocks under mixed-mode loading is important in rock engineering. First, a new configuration called the notched deep beam (NDB) specimen was introduced for the fracture testing of rock materials under mixed-mode I/II loading, and a series of finite element analyses were performed to calibrate the dimensionless fracture parameters (i.e., Y_I , Y_{II} and T^*). The results showed that an NDB specimen subjected to three-point bending is able to generate pure mode I loading, pure mode II loading, and any mixed-mode loading in between. Then, several NDB specimens made of sandstone were used to investigate the brittle fracture behavior of rock under mixed-mode I/II loading. The fracture surfaces were theoretically described using a statistical method, and the results indicated that all the fracture surfaces generated under different mixed-mode loading were statistically identical; to some extent, these results experimentally showed that only tensile fracture occurs under mixed-mode I/II loading. The obtained fracture strengths were then analyzed using several brittle fracture criteria. The empirical criterion, maximum energy release rate criterion, generalized maximum tangential stress (GMTS) criterion, and improved R -criterion accurately predicted the fracture strength envelope of the sandstone. Finally, based on the concepts of point stress and mean stress, the micro-crack zones (MCZs) under different mixed-mode loading were

theoretically estimated based on the MTS and GMTS criteria. The critical radius of MCZ in the crack propagation direction was not a constant for all mixed-mode loading conditions regardless of whether the T -stress was considered. This result suggests that the size of the core region used to predict the crack initiation direction and fracture strength based on the GMTS criterion should be chosen more carefully.

Keywords Mixed-mode loading · Notched deep beam specimen · Fracture strength · Fracture surface · Micro-crack zone

List of symbols

| | |
|----------------------|--|
| a | Crack length |
| B | Thickness of an NDB specimen |
| C | $= 1/(2\pi)$ for the PS case, $= 2/\pi$ for the MS case |
| d | Half-distance between the two bottom supports for an NDB specimen |
| E | Young's modulus of elasticity |
| f_1, f_2 | Parameters related to the scale of the micro-crack zone |
| G | Energy release rate |
| G_c | Critical energy release rate |
| h_1, h_2, h_3, h_4 | Heights corresponding to the four vertexes of a grid cell on the surface |
| K_I | Mode I stress intensity factor |
| K_{Ic} | Mode I fracture toughness |
| K_{II} | Mode II stress intensity factor |
| K_{IIc} | Mode II fracture toughness |
| L | Length of an NDB specimen |
| P | Applied load in an NDB three-point bending test |

✉ L. Ren
renli-scu@hotmail.com

¹ MOE Key Laboratory of Deep Underground Science and Engineering, School of Architecture and Environment, Sichuan University, Chengdu 610065, China

² Institute of New Energy and Low-Carbon Technology, Sichuan University, Chengdu 610065, China

| | |
|---|---|
| P_{cr} | Peak load in an NDB three-point bending test |
| r, ϑ | Polar coordinates at the crack tip |
| r_0 | Critical radius of the core region in the crack propagation direction |
| r_c | Radius of the core region |
| $R_{II,I}$ | Fracture toughness ratio |
| r_p | Elastic–plastic boundary radius |
| r_{pc} | Critical elastic–plastic boundary radius |
| S | Strain energy density factor |
| S_c | Critical strain energy density factor |
| T | Nonsingular stress term |
| T^* | Nondimensional nonsingular stress term |
| W | Width of an NDB specimen |
| Y_I | Nondimensional mode I stress intensity factor |
| Y_{II} | Nondimensional mode II stress intensity factor |
| α | Crack inclination angle for an NDB specimen |
| β_I, β_{II} | Empirical parameters of the empirical criterion |
| δ | Scale of each grid cell |
| η_I, η_{II} | Parameters of the loading mode mixity |
| κ | = 3 – 4 ν for the plane strain case, = (3 – ν)/(1 + ν) for the plane stress case |
| ν | Poisson’s ratio |
| μ | Shear modulus |
| ζ | = 2(1 – 2 ν^*)/3; $\nu^* = \nu$ for the plane strain case, $\nu^* = 0$ for the plane stress case |
| $\sigma_{rr}, \sigma_{\vartheta\vartheta}, \sigma_{r\vartheta}$ | Stress components in polar coordinates |
| σ_t | Tensile strength of a given material |
| $\sigma_{xx}, \sigma_{yy}, \sigma_{xy}$ | Stress components in Cartesian coordinates |
| $\sigma_{\vartheta\vartheta c}$ | Critical tangential stress |

1 Introduction

Fractures are very common in various rock engineering applications, including coal mining, blasting, tunnel excavation, and hydraulic fracturing in unconventional gas exploitation (Chang et al. 2002). For instance, coal mining can redistribute local stresses in the surrounding rock mass, which ultimately leads to mining-induced fractures (Zhang et al. 2013, 2015). Due to the complex in situ stresses and arbitrary orientations of rock fractures, both pre-existing and newly generated fractures are usually subjected to mixed-mode loading rather than pure mode loading. For instance, under the influences of far-field in situ stresses and perforation orientations, a hydraulic fracture usually bears mixed-mode loading and will reorient itself during fracture propagation as the fracture extends from the

wellbore to align with the preferred direction for fracture growth relative to the far-field stresses (Zhang et al. 2011). However, several important issues regarding rock fracturing under mixed-mode loading have yet to be addressed. Addressing these issues will allow significant progress to be achieved in understanding the fracture mechanism under mixed-mode loading and can improve the application of rock fracture mechanics in rock engineering.

The tensile strength of brittle rocks is generally much smaller than their compressive strength and shear strength. Consequently, fracture toughness tests are usually subjected to compressive loads in which tensile stresses are induced (Chong and Kuruppu 1984). Currently, several specimen configurations are frequently used for mixed-mode fracture toughness tests, including the cracked chevron-notched Brazilian disk (CCNBD) specimen (Dai et al. 2014; Fowell 1995; Sheity et al. 1985), the centrally cracked circular disk (CCCD, also known as CSTBD) specimen (Atkinson et al. 1982; Awaji and Sato 1978), the semicircular bend (SCB) specimen containing an edge crack (Chong and Kuruppu 1984; Dai et al. 2010; Funatsu et al. 2014; Lim et al. 1994; Ren et al. 2014), the chevron-notched semicircular bend (CNSCB) specimen (Kuruppu 1997), the cracked straight through flattened Brazilian disk (CSTFBD) specimen (Wang et al. 2011), and the recently proposed edge cracked triangular (ECT) specimen subjected to three-point bending (Aliha et al. 2013). Among these specimens, the International Society for Rock Mechanics (ISRM) has recommended the CCNBD and SCB specimens as the standard configurations for testing the mode I fracture toughness of rocks. Notably, all the specimens mentioned above have simple configurations and loading setups, require inexpensive preparation, and offer the ability to introduce all possible combinations of mode I and II loading. Because disk-type specimens are typically machined from a rock core, some difficulties may arise when preparing circular or disk samples with very large size (Aliha et al. 2013). Unlike circular disk-type specimens, ECT samples of any desired size can be easily obtained via simple cutting from rock blocks (Aliha et al. 2013). This paper proposes a novel configuration, namely the notched deep beam (NDB) specimen, for testing the mixed-mode fracture toughness of rock materials. Numerical analyses demonstrate that the NDB specimen can be used to test the mixed-mode fracture toughness of rocks under a full range of mode mixities, from pure mode I to pure mode II. Similar to the SCB and ECT specimens, the NDB specimen achieves this range through different combinations of the crack inclination angle α , the crack length a and the half-distance d between the two bottom supports. Moreover, NDB specimens of any size can be easily obtained via simple cutting from rock blocks, similar to ECT specimens.

During the rupture of a rock, complex rough fracture surfaces are generated as a result of the irregular grainy features of the material (Ai et al. 2014). Insight into the topographical characteristics of the fracture surface, especially a quantitative description, is significant for better understanding the micro-failure mechanism (Zhou and Xie 2003). The fracture pattern under mixed-mode I/II loading has been identified as tensile fracture (Backers 2005; Backers and Stephansson 2012; Rao et al. 2003). However, this conclusion requires experimental clarification. Recently, using a fractal method, Ren et al. (2016) conducted a series of surface topography measurements of fracture surfaces obtained in mixed-mode I/II fracture tests on SCB specimens made of sandstone. Their investigation indicated that at least on a scale of millimeters, the investigated fracture surfaces were statistically similar. Based on this result, it was concluded that the fracture pattern observed in a mixed-mode I/II fracture test would always correspond to the tensile mode. However, the SCB specimens used in that study were very small, with a radius of 25 mm, and the grain size was relatively large (almost 1 mm in diameter). Therefore, the surface area that could be addressed in that study was limited, and the conclusion regarding the fracture pattern requires further examination. Therefore, the verification of the fracture pattern under mixed-mode I/II loading remains incomplete. To address this shortcoming, this study uses a statistical method to theoretically describe the fracture surfaces of large NDB specimens produced under different loading mixities.

In fracture theory, it is desirable to have a reliable and general fracture criterion that is able to predict both fracture load and growth direction under mixed-mode loading. The linear elastic fracture mechanics (LEFM) criteria have been extensively investigated, and many fracture criteria have been proposed for predicting brittle fracture under mixed-mode I/II loading, such as the maximum tangential stress (MTS) criterion (Erdogan and Sih 1963), a modified version of the MTS criterion (Khan and Khraisheh 2000), the minimum strain energy density (MSED) criterion (Sih 1974), the maximum energy release rate (MERR) criterion (Palaniswamy and Knauss 1972), the T -criterion (Theocaris and Andrianopoulos 1983), the M -criterion (Kong et al. 1995), and the maximum dilatational strain energy density criterion (Yehia and Shephard 1987). To better predict brittle fracture strength under mixed-mode loading, several researchers have proposed a nonlocal theory by incorporating T -stress into the original MTS criterion, which is now known as the generalized maximum tangential stress (GMTS) criterion (Seweryn 1998; Smith et al. 2006). Further examinations of the GMTS criterion have been performed and

have confirmed that considering T -stress in the MTS criterion can indeed improve the mixed-mode fracture strength predictions for rock materials (Aliha and Ayatollahi 2011; Ayatollahi and Aliha 2007a). It should be noted that all the criteria mentioned above use a constant radius to determine the crack initiation angle and fracture strength and that the value of this constant radius does not affect the predictions for most of these criteria (Ren et al. 2013b). However, for the GMTS criterion, the value of the critical radius has a clear influence on the predicted initiation direction and fracture load (as shown later in this paper). By contrast, Mróz and Mróz (2010) used a variable critical radius to establish the MK -criterion; the variable critical radius is defined with respect to the damage zone related to the hydrostatic portion of the total strain energy and can be obtained by combining the critical radii corresponding to pure mode I and pure mode II loading conditions. Similarly, based on the R -criterion proposed by Khan and Khraisheh, Ren et al. (2013a) used a convex combination of the mode I and mode II critical plastic radii to determine the fracture load under mixed-mode loading for an elastic–plastic material (2004), thus proposing the improved R (IR)-criterion. Both the MK -criterion and the IR -criterion have been experimentally verified to be reliable for predicting brittle fracture under mixed-mode loading. Two significant issues should be seriously discussed: (1) whether the critical radius of the core region (which may be determined based on a specified failure theory, e.g., the maximum tensile stress theory) in the crack propagation direction remains constant and (2) how the critical radius affects the theoretical predictions of a criterion that assumes a constant radius. This paper investigates the applicability of several of the above-mentioned criteria for brittle rocks by comparing the results predicted by these criteria with test data of NDB specimens made of sandstone. Based on the concepts of the point stress (PS) and mean stress (MS), theoretical estimates of the micro-crack zones (MCZs) that form under different mixed-mode loading are considered to address these issues.

2 Brief Review of the Stresses Around a Crack Tip in a Cracked Body

The stress field around a crack tip is the basis for analyzing the fracture behavior of a cracked structure and establishing a fracture criterion. According to Williams (1957), the in-plane stress field of a point near the crack tip in a Cartesian coordinate system (x, y) in the plane case can be expressed as follows:

$$\begin{aligned}
 \sigma_{xx} &= \frac{1}{\sqrt{2\pi r}} \left[K_I \cos \frac{\vartheta}{2} \left(1 - 2 \sin \frac{\vartheta}{2} \sin \frac{3\vartheta}{2} \right) - K_{II} \sin \frac{\vartheta}{2} \left(2 + \cos \frac{\vartheta}{2} \cos \frac{3\vartheta}{2} \right) \right] + T \\
 \sigma_{yy} &= \frac{1}{\sqrt{2\pi r}} \left[K_I \cos \frac{\vartheta}{2} \left(1 + 2 \sin \frac{\vartheta}{2} \sin \frac{3\vartheta}{2} \right) + K_{II} \sin \frac{\vartheta}{2} \cos \frac{\vartheta}{2} \cos \frac{3\vartheta}{2} \right] \\
 \sigma_{xy} &= \frac{1}{\sqrt{2\pi r}} \left[K_I \cos \frac{\vartheta}{2} \sin \frac{\vartheta}{2} \cos \frac{3\vartheta}{2} + K_{II} \cos \frac{\vartheta}{2} \left(1 - \sin \frac{\vartheta}{2} \sin \frac{3\vartheta}{2} \right) \right],
 \end{aligned}
 \tag{1}$$

where r and ϑ are the polar coordinates of a point, for which the origin is defined as the crack tip; K_I and K_{II} are the mode I and mode II stress intensity factors, respectively; and T is a nonsingular term called the T -stress, which is parallel to stress σ_{xx} . The stress field around a crack tip can then be written in polar coordinates (r, ϑ) as follows:

$$\begin{aligned}
 \sigma_{rr} &= \frac{1}{\sqrt{2\pi r}} \left[\frac{K_I}{4} \left(5 \cos \frac{\vartheta}{2} - \cos \frac{3\vartheta}{2} \right) - \frac{K_{II}}{4} \left(5 \sin \frac{\vartheta}{2} - 3 \sin \frac{3\vartheta}{2} \right) \right] + T \cos^2 \vartheta \\
 \sigma_{\vartheta\vartheta} &= \frac{1}{\sqrt{2\pi r}} \left[\frac{K_I}{4} \left(3 \cos \frac{\vartheta}{2} + \cos \frac{3\vartheta}{2} \right) - \frac{K_{II}}{4} \left(3 \sin \frac{\vartheta}{2} + 3 \sin \frac{3\vartheta}{2} \right) \right] + T \sin^2 \vartheta \\
 \tau_{r\vartheta} &= \frac{1}{\sqrt{2\pi r}} \left[\frac{K_I}{4} \left(\sin \frac{\vartheta}{2} + \sin \frac{3\vartheta}{2} \right) + \frac{K_{II}}{4} \left(\cos \frac{\vartheta}{2} + 3 \cos \frac{3\vartheta}{2} \right) \right] - T \sin \vartheta \cos \vartheta.
 \end{aligned}
 \tag{2}$$

Considering only the singular stresses in a fracture criterion was once believed to be sufficient. However, Smith et al. (2006) noted that the nonsingular T -stress can also affect crack initiation. Therefore, T and the stress intensity factors K_I and K_{II} are the three important factors for predicting brittle fracture under mixed-mode loading (Aya-tollahi and Aliha 2007b).

3 NDB Bending Method for Fracture Testing Under Mixed-Mode I/II Loading

3.1 Fracture Parameters at the Crack Tip in the NDB Specimen

The proposed test configuration for the NDB specimen is a brick-type rectangle with a length-to-width ratio (L/W) of 2.0, an inclined edge crack of length a , and an angle of α relative to the loading direction, as shown in Fig. 1. The NDB specimen is subjected to a vertical load P under symmetrical three-point bending, and the distance between the bottom supports of the loading fixture is $2d$. NDB samples can be easily made by simply cutting them from

rock blocks; no drilling is necessary. Pure mode I, pure mode II, and any intermediate mixed-mode loading conditions can be achieved by employing different combinations of the crack length a , the crack inclination angle α , and the half-span distance d , as shown in the following section.

Similar to the variables in an SCB or ECT specimen subjected to symmetrical three-point bending, the stress intensity factors K_I and K_{II} and the T -stress in the NDB specimen can be written as functions of the geometric parameters and the applied load, i.e.,

$$Y_I \left(\frac{a}{W}, \frac{d}{W}, \alpha \right) = \frac{K_I}{\sqrt{\pi a}} \frac{2WB}{P},
 \tag{3}$$

$$Y_{II} \left(\frac{a}{W}, \frac{d}{W}, \alpha \right) = \frac{K_{II}}{\sqrt{\pi a}} \frac{2WB}{P},
 \tag{4}$$

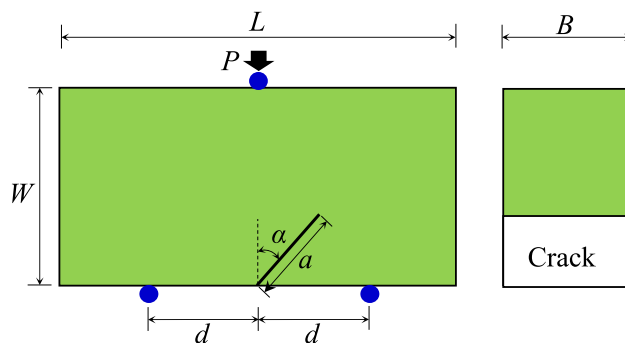


Fig. 1 Notched deep beam (NDB) specimen

$$T^* \left(\frac{a}{W}, \frac{d}{W}, \alpha \right) = T \frac{2WB}{P}, \quad (5)$$

where P is the applied load, B is the thickness of the NDB specimen, Y_I and Y_{II} are the mode I and mode II nondimensional stress intensity factors, respectively, and T^* is the nondimensional form of the T -stress. The three geometrical parameters, Y_I , Y_{II} , and T^* , depend on the crack length ratio (a/W), the loading span ratio (d/W), and the crack inclination angle α . When the crack angle α is zero, the specimen is subjected to pure mode I loading. With increasing angle α , the mode II deformation intensifies. Pure mode II fracture ($Y_I = 0$) occurs at a specific angle α that depends on a/W and d/W .

3.2 Numerical Calibration of the Fracture Parameters of NDB Specimens

To calculate the nondimensional parameters Y_I , Y_{II} , and T^* , several numerical models of NDB specimens were established using the finite element model (FEM) code Abaqus. The Young's modulus E and Poisson's ratio ν were set to 3.90 GPa and 0.26, respectively, and the material was assumed to behave in a linear elastic manner. The length L , width W , and thickness B of each NDB specimen were set to 180, 90, and 76 mm, respectively. The displacement in the Y direction was constrained to zero for the two bottom supports, and the displacement in the X direction for the left bottom support was also set to zero. A reference load of $P = 30$ kN was applied at the upper loading point. A singular 6-node quadratic plane strain triangle element type (CPE6) was used for the first ring of elements around the crack tip, and an 8-node biquadratic plane strain quadrilateral element type (CPE8) was employed for the other elements. To smooth the curves of the J -integral paths, 20 rings of quadrilateral elements (36 elements for each ring) around the crack tip were meshed using the sweep technique. Figure 2 shows a typical finite element mesh.

In the numerical models, the crack inclination angle α varied in 5° increments from 0° to 60° ; the crack length ratios (a/W) were 0.4, 0.5, and 0.6; and the support span

ratio (d/W) varied from 0.5 to 0.8 with an increment of 0.1. Figures 3, 4, and 5 show the variations in the dimensionless factors Y_I , Y_{II} , and T^* with α , respectively, for different crack length ratios in the modeled NDB specimens. Figures 3 and 4 show that when the crack inclination angle α is 0° , $Y_I > 0$ and $Y_{II} = 0$, i.e., the crack is subjected to pure mode I (opening mode) loading independent of a/W . As the angle α increases, Y_I decreases, whereas Y_{II} initially increases and then decreases. For a given crack angle α , the value of Y_I increases as d/W increases. Specifically, assuming that the angle α_{II} corresponds to pure mode II loading in the NDB specimen, a crack angle α_{II} that results in $Y_I = 0$ and $Y_{II} \neq 0$ can usually be found for a given combination of a/W and d/W . In other words, NDB specimens can be used to test the mixed-mode fracture toughness of a material over a full range of mode mixities from pure mode I to pure mode II. When $\alpha > \alpha_{II}$, Y_I will be negative, and the loading condition will correspond to the compression shear mode. As shown in Table 1, α_{II} increases as the crack length ratio a/W decreases or as the loading span ratio d/W increases. Specifically, for a small a/W and a large d/W , pure mode II loading may not be achieved. Thus, one should use a relatively long crack and a short support span to guarantee the realization of mode II loading. Figure 5 shows that the normalized T -stress, T^* , increases with increasing α .

4 Fracture Tests of Sandstone Under Various Mixed-Mode Loadings

4.1 Sample Preparation

Visual inspections indicated that the tested material, a typical sandstone, was continuous, homogeneous, and gray in color. In addition, X-ray diffraction (XRD) analysis (see Fig. 6) indicated that the rock was mainly composed of low albite ($\text{NaAlSi}_3\text{O}_8$) and quartz (SiO_2). According to 2 sets of uniaxial compression tests and direct tensile tests, the sandstone had an elastic modulus

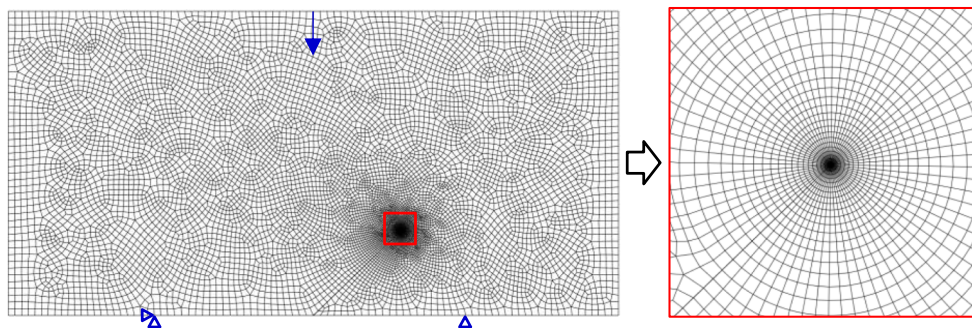


Fig. 2 Typical finite element mesh for an NDB specimen

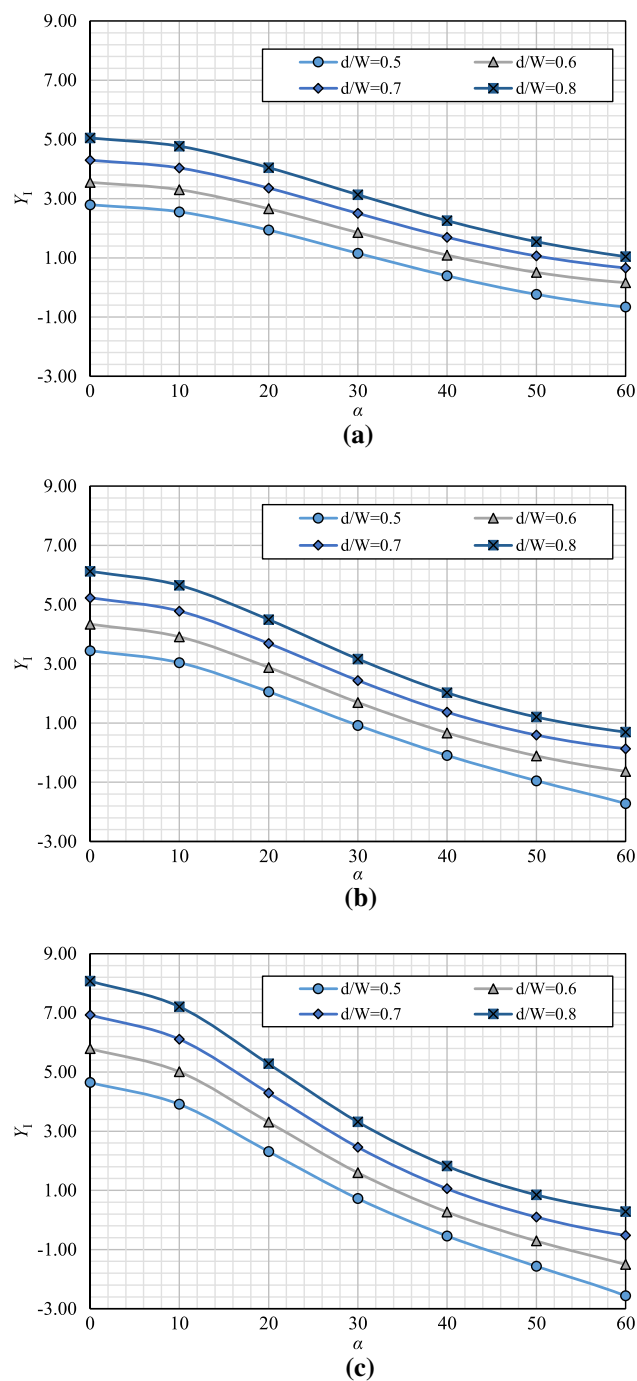


Fig. 3 Variations in Y_I with α among the modeled NDB specimens. **a** $a/W = 0.4$, **b** $a/W = 0.5$, **c** $a/W = 0.6$

E of 3.90 GPa, a Poisson's ratio ν of 0.26, a uniaxial compressive strength σ_c of 16.65 MPa and a direct tensile strength σ_t of 3.37 MPa.

To avoid any possible boundary effects, all specimens were taken from the center of an intact sandstone block. The NDB specimens were large in size, with a length of 180 mm, a width of 90 mm, and a thickness of 76 mm.

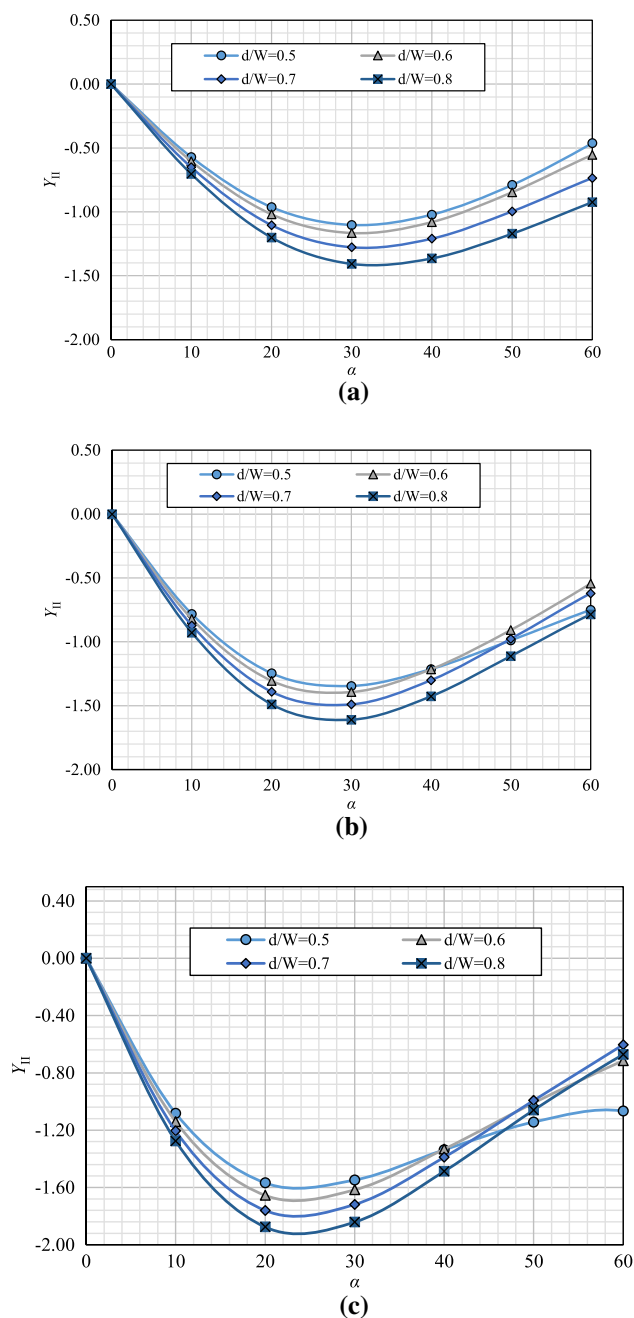


Fig. 4 Variations in Y_{II} with α among the modeled NDB specimens. **a** $a/W = 0.4$, **b** $a/W = 0.5$, **c** $a/W = 0.6$

Values of $d/W = 0.5$ and $a/W = 0.4$ were selected for all specimens. First, cutting and grinding machines were employed to manufacture the NDB specimens. During this process, it is very important to keep any two adjacent faces of the specimen perpendicular to each other. An extremely thin (0.5 mm in thickness) fret saw blade was then used to create edge cracks in the NDB specimens at the required inclination angles. The inclination angle α corresponding to pure mode II loading for this specimen size is

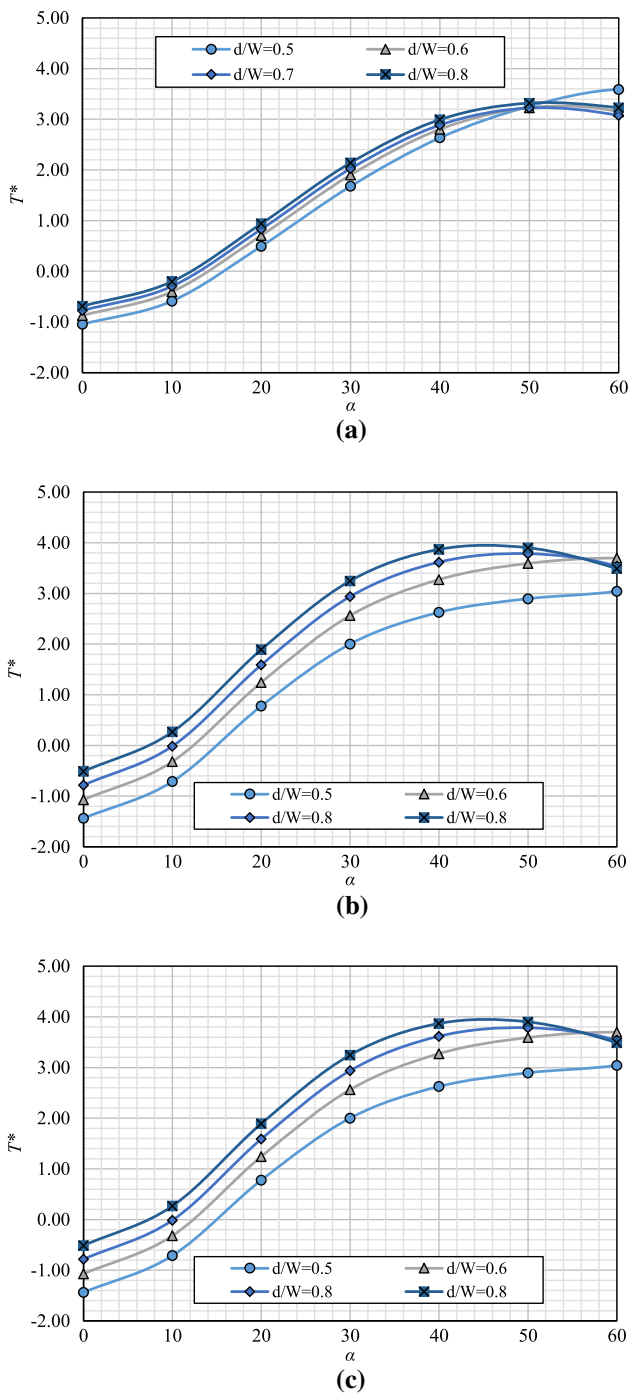


Fig. 5 Variations in T^* with α among the modeled NDB specimens. **a** $a/W = 0.4$, **b** $a/W = 0.5$, **c** $a/W = 0.6$

approximately 45.92° . Therefore, five different crack inclination angles were selected: $\alpha = 0^\circ$ (pure mode I), 10° , 20° , 30° , and 45.9° (pure mode II). A total of 19 NDB specimens were manufactured; five specimens each were tested for the crack angles of 0° and 45.9° , and three specimens each were tested for the crack angles 10° , 20° , and 30° .

Table 1 Values of α_{II} corresponding to various combinations of a/W and d/W for NDB specimens

| | $d/W = 0.5$ | $d/W = 0.6$ | $d/W = 0.7$ | $d/W = 0.8$ |
|-------------|--------------|--------------|--------------|-------------|
| $a/W = 0.4$ | 45.9° | Null | Null | Null |
| $a/W = 0.5$ | 39.0° | 48.4° | 67.1° | Null |
| $a/W = 0.6$ | 35.4° | 42.4° | 51.3° | Null |

4.2 Mixed-Mode Fracture Tests

The MTS 815 Rock Mechanics Test System was employed for mixed-mode fracture testing, and the loading rate for all specimens was set to a constant displacement value of 0.03 mm/min to guarantee quasi-static loading. For all tests, the axial loading was controlled by a linear variable differential transformer (LVDT) sensor with a high accuracy of 0.0002%. The specimens were placed inside a three-point bending fixture, as shown in Fig. 7, and all specimens were tested at room temperature. The half-distance d between the two bottom supports was 45 mm.

The failure patterns of the NDB specimens under different mixed-mode loading conditions are presented in Fig. 8. This figure shows that in all the specimens, cracking initiated from the original crack tip and then propagated through the specimen toward the upper loading point. Under pure mode I loading ($\alpha = 0^\circ$), the crack extended straight along the original crack plane. Under mixed-mode or pure mode II loading, the fracture path was curvilinear and deviated from the original crack line more distinctly with a larger crack angle α .

Figure 9 presents typical plots of the load versus the displacement under different loading conditions. For a larger crack inclination angle, the peak load shows a longer delay, i.e., the displacement required to induce a macro-fracture increases. The load–displacement curves instantaneously decreased after reaching the peak values, indicating the brittle behavior of the tested rock. The peak loads F_{cr} measured from the tests—except that of specimen #30-1, which was destroyed during the preloading process because of operator error—are listed in Table 2. The critical load gradually increased as the proportion of mode II loading increased. The peak load P_{cr} is the parameter that is required to determine the mixed-mode fracture toughness of an NDB specimen. The critical stress intensity factors, namely the mixed-mode fracture toughness of the sandstone and the critical T -stress, can be calculated by substituting the measured peak load P_{cr} for the applied load P in Eqs. (3), (4), and (5); the results of these calculations are also presented in Table 2. The mode I and mode II fracture toughnesses K_{Ic} and K_{IIc} were obtained by calculating the average critical stress intensity factors for the NDB specimens with crack angles of 0° and 45.9° and were found to be 0.378 and $0.234 \text{ MPa m}^{1/2}$, respectively.

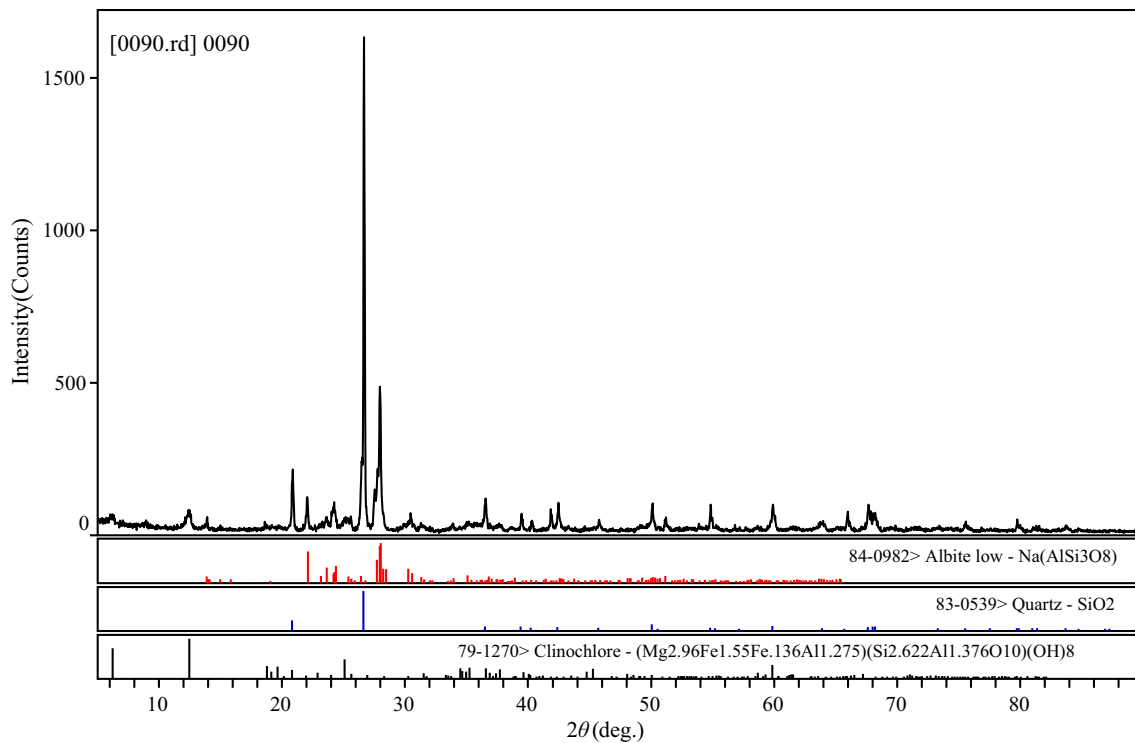
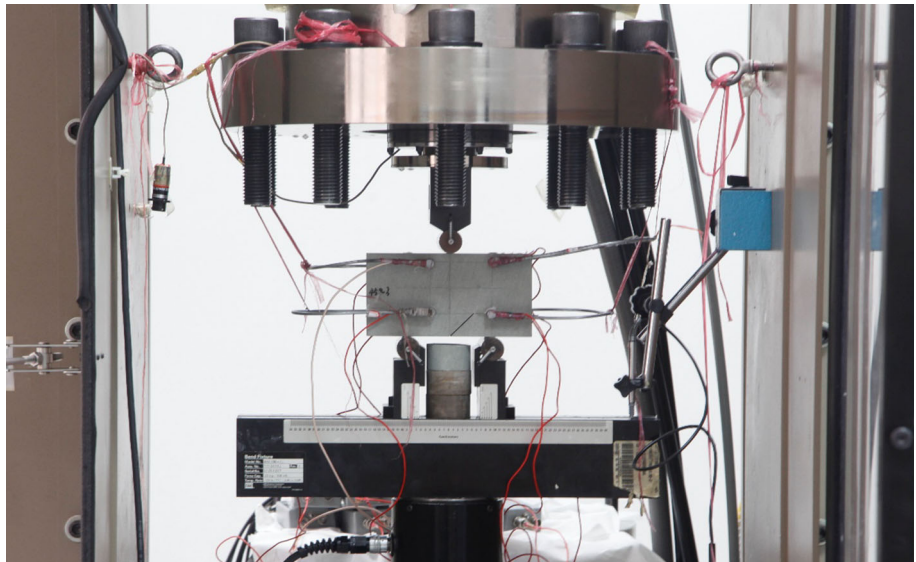


Fig. 6 XRD results for the tested sandstone

Fig. 7 Loading device and an NDB specimen



Therefore, the fracture toughness ratio K_{IIc}/K_{Ic} is approximately 0.62 for the tested sandstone.

5 Topographical Characteristics of Fracture Surfaces

A quantitative description of the fracture surface topography can provide a better understanding of the micro-failure mechanism of the tested sandstone. Babadagli and Develi

(2003) indicated that the petrological–mineralogical and petrophysical properties of a rock sample exert a strong influence on the roughness of its fracture surface. In this study, all the NDB samples were collected from a single enormous block of rock; thus, it was reasonable to analyze the topographical characteristics of their fracture surfaces depending on the loading mixity. A noncontact 3D laser profilometer was employed to measure the fracture surfaces of the NDB specimens. This laser probe had an elevation range of 300 mm with an accuracy of ± 0.1 mm. A

Fig. 8 Failure patterns of the sandstone NDB specimens. **a** $\alpha = 0^\circ$, **b** $\alpha = 10^\circ$, **c** $\alpha = 20^\circ$, **d** $\alpha = 30^\circ$, **e** $\alpha = 45.9^\circ$

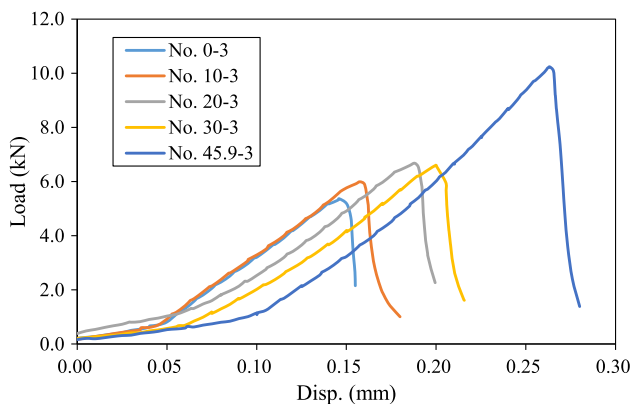
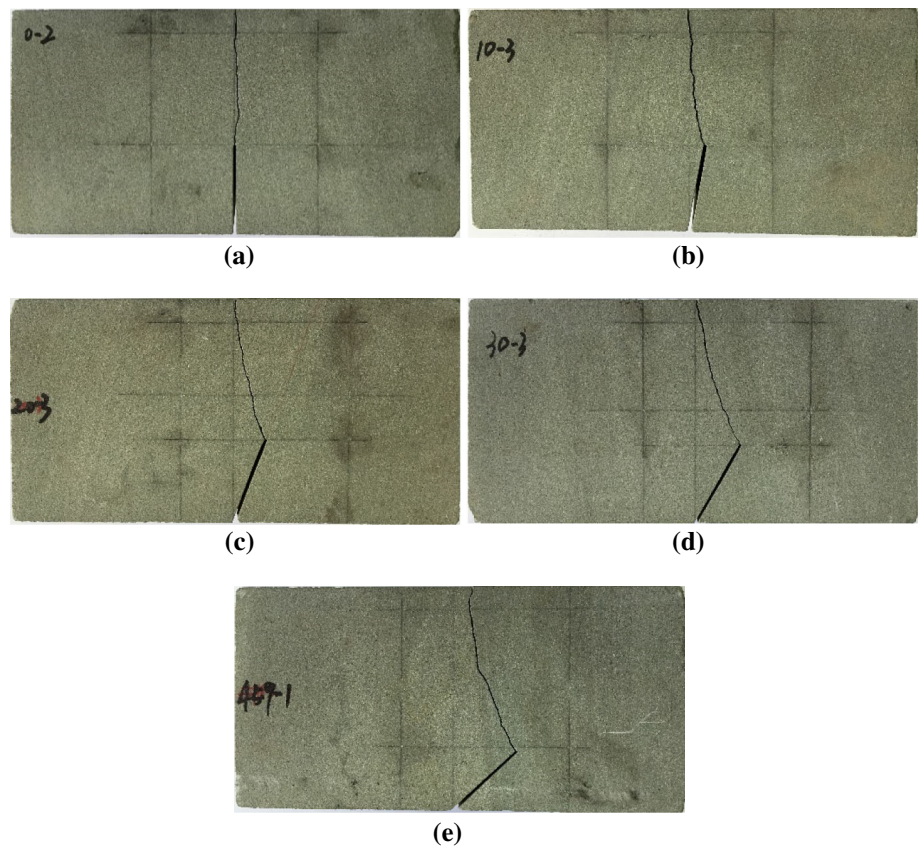


Fig. 9 Load–displacement curves of the NDB specimens with different crack inclination angles

measured data file from the fracture surface comprised both the planar coordinates (x and y coordinates) of the scanning field and the corresponding height (z coordinate) of the measured point. For each sample, the fracture surface was scanned within a $48 \text{ mm} \times 48 \text{ mm}$ area ahead of the crack tip along the crack propagation path. The sampling interval for each fracture surface was set to a constant value of 0.1 mm ; therefore, a total of 480×480 sampling points was used to reconstruct the isometric view of the fracture surface of each NDB specimen. The reconstructed fracture

surface profile views corresponding to different mixed-mode loading conditions are illustrated in Fig. 10. This figure clearly shows that it is difficult to distinguish the fracture surfaces generated under various loading mixities simply through visual inspection.

A statistical analysis was performed to mathematically describe the fracture surfaces. As shown in Fig. 11, a regular square grid was assumed to exist on the reference plane XOY , and the scale of each grid cell was taken to be δ . In each grid cell, four heights, namely $h_1(i, j)$, $h_2(i, j + 1)$, $h_3(i + 1, j)$, and $h_4(i + 1, j + 1)$, define the four vertices of the corresponding surface, where i and j are the numbers of the grid cell in the X and Y directions, respectively, such that $1 \leq i, j \leq n - 1$, where n is the total number of sampling points in each direction on the fracture surface. The maximum difference $\Delta h(i, j)$ among the four heights in each grid cell was calculated using the following equation:

$$\Delta h(i, j) = \max(h_1, h_2, h_3, h_4) - \min(h_1, h_2, h_3, h_4). \quad (6)$$

$\Delta h(i, j)$ reflects the asperity within the (i, j) th surface area, and a steeper asperity corresponds to a larger Δh . Taking sample No. 0-2 as an example, as illustrated in Table 3, shows that the statistical characteristics of Δh vary with the grid cell scale δ . As the measurement scale δ

Table 2 Results of mixed-mode I/II fracture tests on NDB specimens made of sandstone

| Specimen no. | α (°) | P_{cr} (kN) | K_I (MPa m ^{1/2}) | K_{II} (MPa m ^{1/2}) | T -stress (MPa) |
|--------------|--------------|---------------|-------------------------------|----------------------------------|-------------------|
| 0-1 | 0 | 5.360 | 0.368 | 0.000 | -0.409 |
| 0-2 | 0 | 5.845 | 0.401 | 0.000 | -0.446 |
| 0-3 | 0 | 5.366 | 0.368 | 0.000 | -0.410 |
| 0-4 | 0 | 5.607 | 0.385 | 0.000 | -0.428 |
| 0-5 | 0 | 5.345 | 0.367 | 0.000 | -0.408 |
| 10-1 | 10 | 5.926 | 0.372 | 0.083 | -0.255 |
| 10-2 | 10 | 5.688 | 0.357 | 0.080 | -0.245 |
| 10-3 | 10 | 5.99 | 0.376 | 0.084 | -0.258 |
| 20-1 | 20 | 6.107 | 0.291 | 0.145 | 0.221 |
| 20-2 | 20 | 6.626 | 0.316 | 0.157 | 0.239 |
| 20-3 | 20 | 6.675 | 0.318 | 0.158 | 0.241 |
| 30-1 | 30 | – | – | – | – |
| 30-2 | 30 | 7.616 | 0.216 | 0.206 | 0.934 |
| 30-3 | 30 | 6.605 | 0.187 | 0.179 | 0.810 |
| 45.9-1 | 45.9 | 11.304 | 0.000 | 0.250 | 2.512 |
| 45.9-2 | 45.9 | 10.787 | 0.000 | 0.238 | 2.397 |
| 45.9-3 | 45.9 | 10.563 | 0.000 | 0.233 | 2.348 |
| 45.9-4 | 45.9 | 10.234 | 0.000 | 0.226 | 2.274 |
| 45.9-5 | 45.9 | 10.172 | 0.000 | 0.225 | 2.261 |

increases, the average value, standard deviation, and variance increase, whereas the skewness and kurtosis decrease. The measurement scale δ strongly affects both Δh and the statistical characteristics of Δh . Therefore, it was necessary to perform the analysis for all fracture surfaces at a universal measurement scale δ , which was set to 0.1 mm in this study. Table 4 presents the statistical analysis results for each fracture surface generated under different loading mixities. The average values, standard deviations, and variances of all the specimens are very close. The average values lie in a range of 0.5–0.7 mm, and the average value of Δh for each sample is greater than the median. These results indicate that for each NDB specimen, the surface area that possesses an asperity that is steeper than average occupies more than 50% of the entire fracture surface. The skewness and kurtosis reflect the asymmetry and shape of the frequency distribution of Δh , respectively. Positive skewness values indicate that the frequency distribution of the height difference Δh , which is greater than the average value, is more discrete. Kurtosis values of greater than 3.0 reveal that the frequency distribution of Δh is steeper than the standard normal distribution. To some extent, the frequency distributions for the fracture surfaces induced by various mixed-mode loadings are approximate. Figure 12 shows the surface roughness distribution curves for 5 specimens; these curves depict the cumulative frequency versus the height difference Δh . Overall, the differences in the roughness distribution curves among the five groups of NDB specimens are very small. There are differences in

the statistical parameters for each group of NDB specimens, but no clear trend is universally observed between any given statistical parameter and the loading mode mixity. This result is consistent with previous findings (Ren et al. 2016). Moreover, the fracture patterns in Fig. 8 clearly show that after crack initiation, the crack growth was nearly self-similar, i.e., the cracks propagated in a manner dominated by mode I fracture. Therefore, only tensile mode failure occurred in the NDB specimens subjected to mixed-mode I/II loading.

6 Theoretical Prediction of Fracture Strength Using Several Criteria

6.1 Theoretical Review

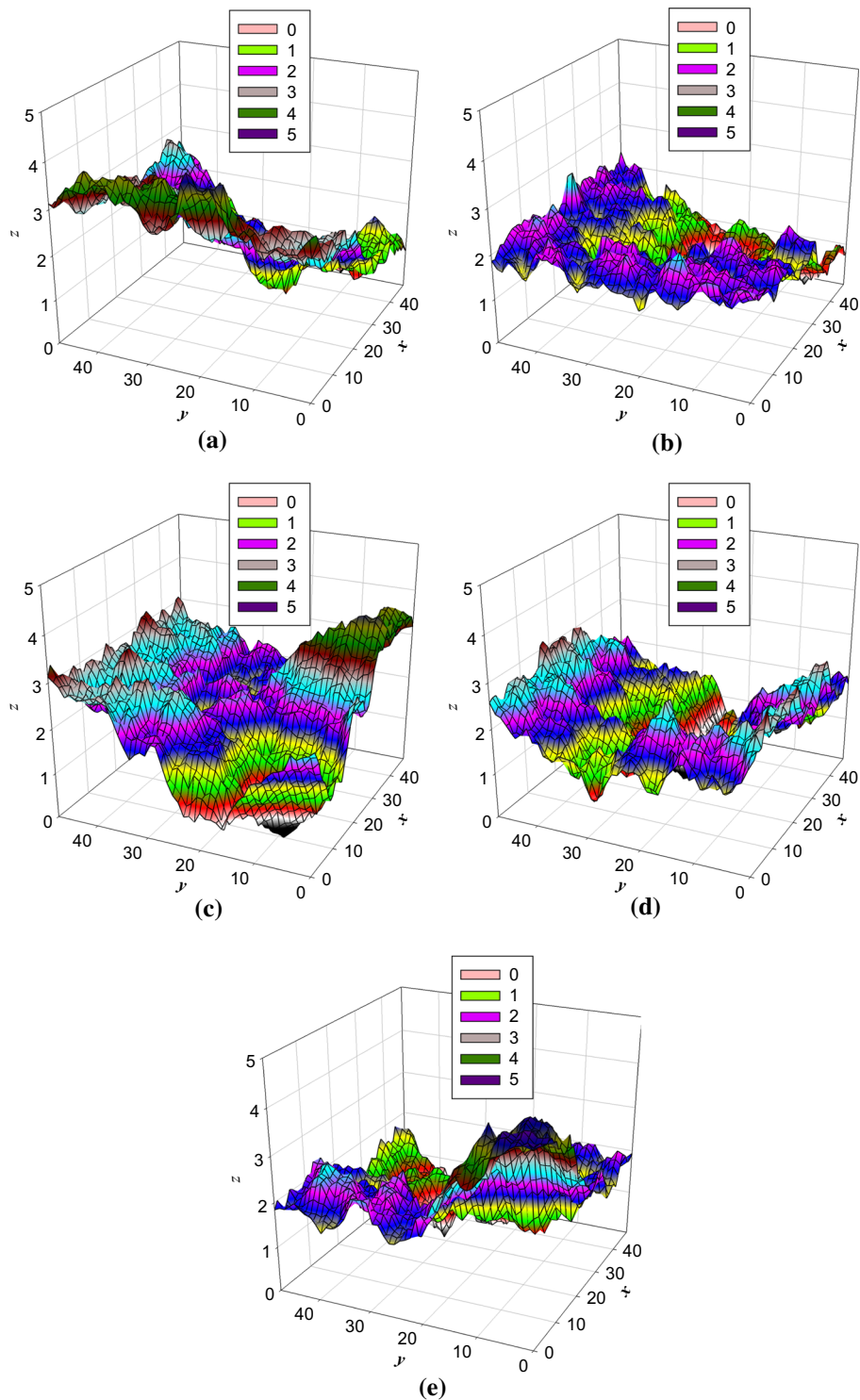
6.1.1 MTS Criterion

The MTS criterion proposed by Erdogan and Sih (1963) assumes that the crack propagation starts along the direction ϑ_0 on which the tangential stress $\sigma_{\vartheta\vartheta}$ becomes maximum and the occurrence of crack initiation once the MTS reaches a critical value $\sigma_{\vartheta\vartheta c}$, i.e.,

$$\frac{\partial \sigma_{\vartheta\vartheta}}{\partial \vartheta} = 0, \quad \frac{\partial^2 \sigma_{\vartheta\vartheta}}{\partial \vartheta^2} < 0 \text{ at } \vartheta = \vartheta_0, \quad \sigma_{\vartheta\vartheta c} = \frac{K_{Ic}}{\sqrt{2\pi r_0}}, \quad (7)$$

where r_0 is the distance from the crack tip to the boundary of the core region along the crack propagation direction.

Fig. 10 Fracture surface topography plots. **a** $\alpha = 0^\circ$, **b** $\alpha = 10^\circ$, **c** $\alpha = 20^\circ$, **d** $\alpha = 30^\circ$, **e** $\alpha = 45.9^\circ$



Regardless of the T -stress term, by substituting Eq. (2) into Eq. (7), r_0 will be eliminated, and the crack initiation angle and critical load can be calculated using the following equations:

$$K_I \sin \vartheta_0 + K_{II}(3 \cos \vartheta_0 - 1) = 0; \tag{8}$$

$$\frac{1}{2} [K_I(1 + \cos \vartheta_0) - 3K_{II} \sin \vartheta_0] \cos \frac{\vartheta_0}{2} = K_{Ic}. \tag{9}$$

Equations (8) and (9) are independent of r_0 . Thus, the value of r_0 does not affect the calculations of the initiation angle and critical load.

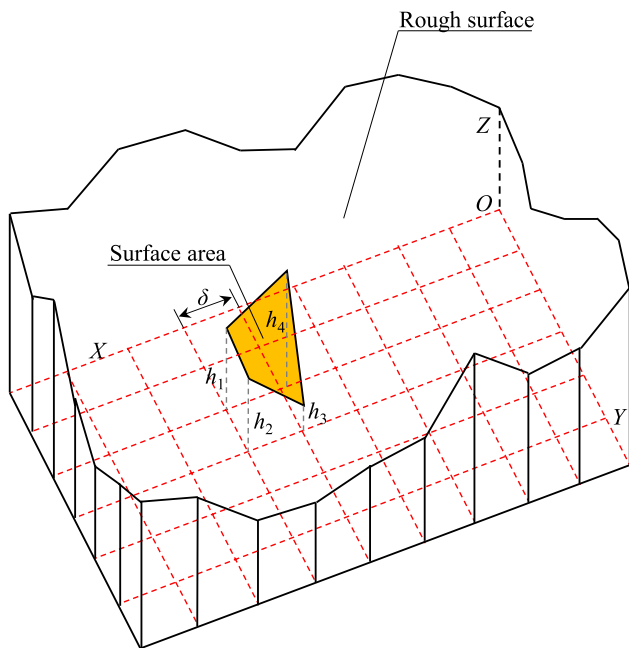


Fig. 11 Schematic view of the heights corresponding to a square grid

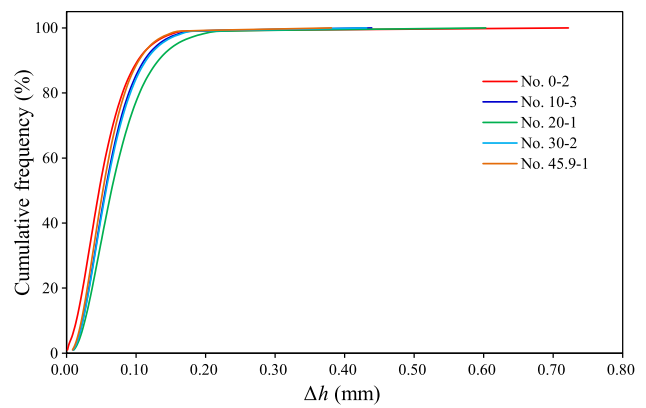


Fig. 12 Cumulative frequency distributions of the surface asperities for various loading modes

6.1.2 GMTS Criterion

The GMTS criterion incorporates the effect of the non-singular T -stress term into the MTS criterion (Smith et al. 2006). When the T -stress term is considered, the tangential stress $\sigma_{\vartheta\vartheta}$ near the crack tip can be written as follows:

Table 3 Statistical parameters of Δh at various measurement scales for sample No. 0-2

| Scale δ (mm) | Average value (mm) | SD | Variance | Skewness | Kurtosis |
|---------------------|--------------------|--------|----------|----------|----------|
| 0.1 | 0.0538 | 0.0367 | 0.0013 | 1.3099 | 6.7752 |
| 0.2 | 0.0946 | 0.0510 | 0.0026 | 1.0743 | 6.9071 |
| 0.3 | 0.1284 | 0.0617 | 0.0038 | 0.9399 | 6.9051 |
| 0.4 | 0.1585 | 0.0717 | 0.0051 | 0.8653 | 6.7715 |
| 0.5 | 0.1859 | 0.0800 | 0.0064 | 0.7345 | 5.4501 |
| 0.6 | 0.2119 | 0.0891 | 0.0079 | 0.7030 | 5.4347 |
| 0.8 | 0.2599 | 0.1054 | 0.0111 | 0.6394 | 5.1046 |
| 1.0 | 0.3036 | 0.1196 | 0.0143 | 0.6210 | 5.1243 |

Table 4 Statistical parameters of Δh for each fracture surface at a measurement scale of 0.1 mm

| Specimen code | Average value (mm) | Median (mm) | SD | Variance | Skewness | Kurtosis |
|---------------|--------------------|-------------|--------|----------|----------|----------|
| 0-2 | 0.0538 | 0.0467 | 0.0367 | 0.0013 | 1.3099 | 6.7752 |
| 0-3 | 0.0463 | 0.0406 | 0.0315 | 0.0010 | 1.0796 | 4.6538 |
| 0-5 | 0.0600 | 0.0526 | 0.0368 | 0.0014 | 1.2406 | 5.5689 |
| 10-1 | 0.0639 | 0.0567 | 0.0371 | 0.0014 | 1.2162 | 5.3074 |
| 10-2 | 0.0604 | 0.0529 | 0.0369 | 0.0014 | 1.3661 | 7.1903 |
| 10-3 | 0.0628 | 0.0557 | 0.0366 | 0.0013 | 1.2383 | 5.5417 |
| 20-1 | 0.0736 | 0.0644 | 0.0451 | 0.0020 | 1.5152 | 7.5199 |
| 20-2 | 0.0548 | 0.0481 | 0.0338 | 0.0011 | 1.4921 | 7.4930 |
| 20-3 | 0.0565 | 0.0500 | 0.0336 | 0.0011 | 1.1742 | 5.1807 |
| 30-2 | 0.0640 | 0.0567 | 0.0375 | 0.0014 | 1.2111 | 5.3407 |
| 30-3 | 0.0589 | 0.0524 | 0.0339 | 0.0011 | 1.1897 | 5.2722 |
| 45.9-1 | 0.0583 | 0.0521 | 0.0337 | 0.0011 | 1.1046 | 4.7389 |
| 45.9-2 | 0.0552 | 0.0489 | 0.0325 | 0.0011 | 1.1286 | 4.7601 |
| 45.9-3 | 0.0656 | 0.0580 | 0.0396 | 0.0016 | 1.4923 | 7.7721 |

$$\sigma_{\vartheta\vartheta} = \frac{1}{\sqrt{2\pi}r_0} \left[\frac{K_I}{4} \left(3 \cos \frac{\vartheta}{2} + \cos \frac{3\vartheta}{2} \right) - \frac{K_{II}}{4} \left(3 \sin \frac{\vartheta}{2} + 3 \sin \frac{3\vartheta}{2} \right) \right] + T \sin^2 \vartheta. \quad (10)$$

When using the GMTS criterion, a suitable value of r_0 should be given in advance. Then, the crack initiation angle and crack propagation condition are calculated using Eq. (7). The value of r_0 will clearly affect the calculation results of both the crack initiation angle and fracture strength. In the GMTS criterion, r_0 is regarded as a constant and can be estimated as

$$r_0 = \frac{1}{2\pi} \left(\frac{K_{Ic}}{\sigma_i} \right)^2. \quad (11)$$

6.1.3 MSED Criterion

The MSED criterion formulated by Sih (1974) is based on the following assumptions: (1) The crack growth takes place in the direction along which the strain energy density factor S possesses a minimum value, and (2) crack propagation occurs when this minimum value reaches a critical value S_c . Then, the MSED criterion can be expressed as

$$\frac{\partial S}{\partial \vartheta} = 0, \quad \frac{\partial^2 S}{\partial \vartheta^2} > 0 \text{ at } \vartheta = \vartheta_0, \quad S_c = \frac{(\kappa - 1)K_{Ic}^2}{8\pi\mu}, \quad (12)$$

where μ is the shear modulus of elasticity and $\kappa = 3 - 4\nu$ for the plane strain problem or $\kappa = (3 - 4\nu)/(1 + \nu)$ for the plane stress case.

6.1.4 MERR Criterion

The MERR criterion proposed by Palaniswamy and Knauss (1972) states that the crack extension will occur along the direction where the energy release rate possesses a maximum value, and when the MERR reaches a critical value G_c . The criterion can be described as

$$\frac{\partial G}{\partial \vartheta} = 0, \quad \frac{\partial^2 G}{\partial \vartheta^2} < 0 \text{ at } \vartheta = \vartheta_0, \quad G_c = \frac{(1 - \nu^2)K_{Ic}^2}{E}. \quad (13)$$

Several forms (Hussain et al. 1974; Kfoury and Brown 1995; Nuismer 1975; Wu 1978) of the MERR have been proposed; the expression formulated by Hussain et al. (1974) is the most widely adopted version.

6.1.5 IR-Criterion

The R -criterion proposed by Khan and Khraisheh (2004) states the direction of the crack initiation angle coincides with the direction of the minimum distance from the crack tip to the elastic–plastic core region boundary, and it can be expressed as

$$\frac{\partial r_p}{\partial \vartheta} = 0, \quad \frac{\partial^2 r_p}{\partial \vartheta^2} > 0 \text{ at } \vartheta = \vartheta_0 \quad (14)$$

The R -criterion clearly employs a variable core region, unlike the above-mentioned fracture criteria. However, the R -criterion cannot predict the fracture load. To address this shortcoming, Ren et al. (2013a) proposed the improved R (IR)-criterion by expressing the critical value r_{pc} of the elastic–plastic boundary radius in the crack growth direction as follows:

$$r_{pc} = 2\sigma\eta_I \xi K_{Ic}^2 + \sigma\eta_{II}(1 + \xi - \xi^2/12)K_{IIc}^2, \quad (15)$$

where η_I and η_{II} are the parameters of the loading mode mixity, i.e.,

$$\eta_I = \frac{K_I K_{IIc}}{K_I K_{IIc} + K_{II} K_{Ic}}, \quad \eta_{II} = \frac{K_{II} K_{Ic}}{K_I K_{IIc} + K_{II} K_{Ic}}. \quad (16)$$

6.1.6 Empirical Criterion

Many researchers have formulated various forms of the empirical criterion (Balzani et al. 2012; Swartz and Taha 1990; Whitcomb 1986; Zhao 1990). The simple elliptic form given by Swartz and Taha (1990) is expressed as

$$\left(\frac{K_I}{K_{Ic}} \right)^{\beta_I} + \left(\frac{K_{II}}{K_{IIc}} \right)^{\beta_{II}} = 1, \quad (17)$$

where reasonable values of β_I and β_{II} are usually calculated through fitting to the experimental data.

6.2 Comparison of the Theoretical Predictions with the Test Results

In this section, the fracture criteria summarized above are employed to theoretically investigate the fracture behavior of the tested sandstone. For the GMTS criterion, the size of the fracture process zone (FPZ), $r_0 = 2$ mm, was theoretically determined using Eq. (10). Figure 13a depicts the theoretical estimates alongside the test results in a plot of K_{II}/K_{Ic} versus K_I/K_{Ic} . This figure clearly shows that the MERR criterion, IR -criterion, and empirical criterion (with $\beta_I = 1.21$ and $\beta_{II} = 3.41$) agree well with the experimental data, whereas the MSED criterion significantly overpredicts the fracture strength of the sandstone even for the loading cases that are dominated by mode I. Under loading conditions that are dominated by mode II, the MTS criterion overestimates the fracture strength of the sandstone, whereas the GMTS criterion (with $r_0 = 2$ mm) underestimates the fracture strength. Figure 13b presents the measured critical loads and the results predicted by these criteria. This figure shows that under pure mode II loading, the critical load predicted by the GMTS criterion with $r_0 = 2.0$ mm is 7.68 kN, which is lower than the experimental result; the MTS criterion yields a larger fracture

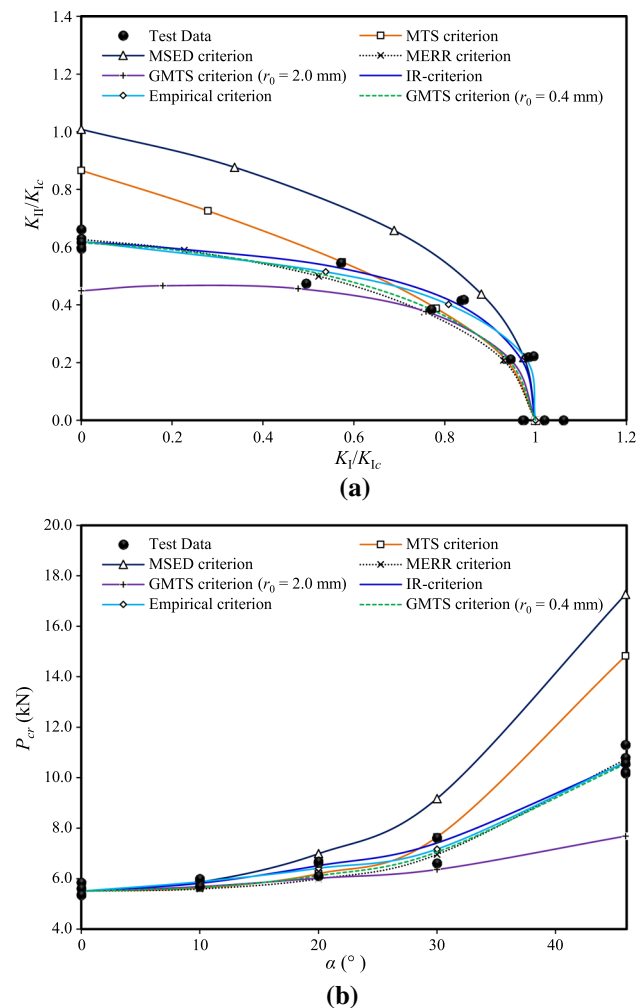


Fig. 13 Comparison of the results predicted by the various fracture criteria and the test results. **a** Fracture envelopes, **b** critical loads versus crack angles

load of 14.82 kN; and the MSED criterion gives a value of 17.26 kN, which is much larger than the test result. In fact, it has been demonstrated that the classical LEFM criterion with a constant core region may fail to predict the fracture strength envelope of a given material. Khan and Khraisheh (2004) noted that from a mathematical point of view, if a constant radius is used in a conventional LEFM criterion that employs a singular elastic stress field, then the value of the core region radius does not influence the crack initiation angle. A later study reported that the dimension of core region radius does not influence the fracture toughness envelope (Ren et al. 2013a). Consequently, the MTS, MSED, and MERR criteria predict invariant fracture toughness ratios of 0.87, $\sqrt{[3(1-2\nu)]/[2(1-\nu)-\nu^2]}$ and 0.63, respectively. However, for different rocks, the fracture toughness ratios may differ. For instance, the fracture toughness ratio K_{IIc}/K_{Ic} of limestone is 0.74 (Hasanpour and Choupani 2009);

consequently, the MERR criterion fails to predict the fracture loads of limestone for loading conditions dominated by mode II (Ren et al. 2016) despite providing good estimates for the sandstone tested in the current study. Therefore, these classical criteria cannot accurately estimate the fracture strength of an arbitrarily chosen material. By contrast, the empirical criterion uses both K_{Ic} and K_{IIc} and is therefore able to provide a better fitting to the experimental data (see Fig. 13). Similarly, both K_{Ic} and K_{IIc} are applied for the IR-criterion, and a variable core region is adopted. Hence, this criterion can also accurately predict the fracture load of a cracked body. Concerning the GMTS criterion, as shown in Fig. 13, the theoretical predictions obtained using $r_0 = 0.4$ mm would exhibit good agreement with the results of the fracture tests instead of 2.0 mm. Obviously, the value of r_0 influences the reliability of the GMTS criterion when predicting the mixed-mode fracture of a brittle rock. Therefore, several values of r_0 will be used to predict the fracture loads. Then, the most suitable value will be adopted; this value does not typically coincide with the theoretical estimation from Eq. (10) but does result in a good estimation of the experimental results (Ayatollahi et al. 2006).

7 Micro-Crack Zones Under Mixed-Mode I/II Loading

The previous section showed that the size of the core region used in a criterion may strongly affect the fracture strength prediction. The core region can be obtained based on various assumptions. Mróz and Mróz (2010) employed the hydrostatic portion of the total strain energy to define the core region when proposing the MK-criterion; Khan and Khraisheh (2004) used the plastic zone as the core region for an elastic-plastic material when proposing the R-criterion. These two criteria employ a variable core region to investigate fracture behavior under mixed-mode loading. Based on the idea proposed by Schmidt (1980) for rock masses, it can be concluded that a tensile stress-induced micro-crack zone (MCZ) is well suited for describing a core region of a rock fracture under mixed-mode loading. In the MTS and GMTS criteria, as the radius r approaches zero, the tangential stress $\sigma_{\theta\theta}$ tends toward infinity. Consequently, an MCZ induced by $\sigma_{\theta\theta}$ must exist around the rock crack tip, and the size of this MCZ reaches its maximum at the peak load. In particular, the critical radius, $r_0 = [1/(2\pi)](K_{Ic}/\sigma_t)^2$, of the MCZ in the crack propagation direction under pure mode I loading is adopted and treated as a constant in the GMTS criterion for all mixed-mode loading (Aliha and Ayatollahi 2011; Ayatollahi and Aliha 2007a). One aspect of this must be clarified: does the critical radius r_0 of the MCZ determined by $\sigma_{\theta\theta}$ in the crack propagation direction

under pure mode I loading equal that under mixed-mode loading and that under pure mode II loading? If not, it is inappropriate to use a constant value of r_0 to predict the crack initiation angle and fracture load in the MTS and GMTS criteria? To address this issue, it is necessary to further examine the critical radii in the crack growth direction of the MCZ for rocks under various mixed-mode loading, which may be helpful for applying the MTS and GMTS criteria in practice and reaching a clearer understanding of the mixed-mode fracture mechanism of rocks. Based on the above description and consideration, the core region is determined using the MTS and GMTS criteria based on a tangential tensile stress failure model.

Several researchers have assumed that macro-fracture will occur once the mean stress (MS) within the characteristic fracture length exceeds the common maximum capacity of a brittle material (Carpinteri et al. 2009; Leguillon 2002; Luo and Wang 2009; Ritchie et al. 1973; Susmel and Taylor 2008; Wang et al. 2016). According to the MS principle, the characteristic fracture length of a rock in the crack propagation direction can be regarded as the critical radius, r_0 , of the MCZ. Based on the MS concept, the boundary equation for the MCZ, in which the mean value of $\sigma_{\vartheta\vartheta}$ along the radius in the direction ϑ equals the tensile strength of a given rock, can be written as

$$\frac{1}{r_c} \int_{r_c} \sigma_{\vartheta\vartheta} dr = \sigma_t, \quad (18)$$

where $\sigma_{\vartheta\vartheta}$ is the tangential stress corresponding to the peak load. In addition, from the perspective of the point stress (PS), the MCZ boundary can be calculated to correspond to the points where $\sigma_{\vartheta\vartheta}$ is exactly equal to the tensile strength of the rock material. Therefore, according to the MTS criterion, the boundary of the MCZ induced by $\sigma_{\vartheta\vartheta}$ can be determined as follows:

$$r_c = Cf_1(\vartheta), \text{ and } f_1(\vartheta) = \frac{1}{\sigma_t^2} \left[\frac{K_I}{2} \cos \frac{\vartheta}{2} (1 + \cos \vartheta) - \frac{3K_{II}}{2} \sin \frac{\vartheta}{2} (1 + \cos \vartheta) \right]^2, \quad (19)$$

where $C = 1/(2\pi)$ when the PS is used, $C = 2/\pi$ when the MS is used, and K_I and K_{II} are the critical stress intensity factors for fracture under mixed-mode loading, namely the mixed-mode fracture toughness of the rock material. This toughness is a combination of the critical stress intensity factors for fracture under mixed-mode loading rather than a constant, such as the mode I fracture toughness K_{Ic} and mode II fracture toughness K_{IIc} .

To determine the MCZ using the GMTS criterion, the effect of the nonsingular T -stress should be considered. Therefore, the MCZ boundary can then be determined as follows:

$$r_c = Cf_2(\vartheta), \text{ and } f_2(\vartheta) = \frac{\left[\frac{K_I}{2} \cos \frac{\vartheta}{2} (1 + \cos \vartheta) - \frac{3K_{II}}{2} \sin \frac{\vartheta}{2} (1 + \cos \vartheta) \right]^2}{(\sigma_t - T \sin^2 \vartheta)^2}. \quad (20)$$

For the MTS criteria, noting that $C = 1/(2\pi)$ for the PS assumption and $C = 2/\pi$ for the MS concept in Eq. (19), the size of the MCZ determined using MS is four times that estimated using the PS assumption. Similarly, according to Eq. (20), the same conclusion can be reached for the GMTS criteria. According to Eqs. (19) and (20), the critical radius of the MCZ in the crack growth direction, i.e., r_0 , used in the MTS and GMTS criteria can be determined by searching the maximum value of r_c , i.e.,

$$\frac{\partial r_c}{\partial \vartheta} = 0, \quad \frac{\partial^2 r_c}{\partial \vartheta^2} < 0; \text{ and } r_0 = (r_c)_{\vartheta=\vartheta_0} = Cf_i(\vartheta_0), \quad i = 1, 2. \quad (21)$$

In the case of mode I fracture, the crack growth occurs in the direction of the original crack. The maximum radius of the MCZ in the direction $\vartheta_0 = 0^\circ$ can then be calculated using the mode I fracture toughness for both the MTS and GMTS criteria:

$$r_0 = C \left(\frac{K_{Ic}}{\sigma_t} \right)^2, \quad (22)$$

From the PS viewpoint, the value of r_0 in the crack growth direction calculated using Eq. (22) is $r_0 = [1/(2\pi)](K_{Ic}/\sigma_t)^2$, which is widely used for the GMTS criterion.

Noting that C is a constant in Eqs. (19) and (20), only f_1 and f_2 , which are the characteristic MCZ parameters, will be discussed in the following. When the peak load is reached, the mixed-mode fracture toughness and the critical T -stress can be obtained; then, f_1 and f_2 can be determined accordingly. As shown in Fig. 14, according to the MTS criterion, the size of the MCZ of the investigated sandstone under pure mode II loading is much smaller than that under mode I loading. By contrast, for the GMTS criterion, the size of the MCZ under pure mode II loading is much larger than that in pure mode I loading. According to Eq. (21), the values of f_1 and f_2 in the crack propagation direction can be easily calculated; these calculation results are presented in Fig. 14. At inclination angles of $\alpha = 0^\circ$ (pure mode I), 10° , 20° , 30° , and 45.9° (pure mode II), the maximum values of f_1 are 12.57, 13.65, 13.72, 10.81, and 6.45 mm, respectively, and the maximum values of f_2 are 12.57, 13.39, 14.62, 16.56, and 62.83 mm, respectively. When the T -stress is neglected, the critical radius, r_0 , of the MCZ in the crack growth direction initially increases and then decreases with increasing crack inclination angle. When the T -

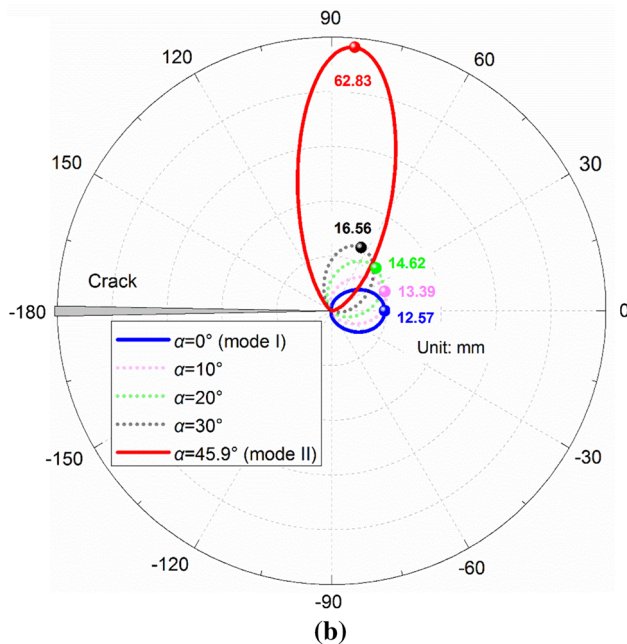
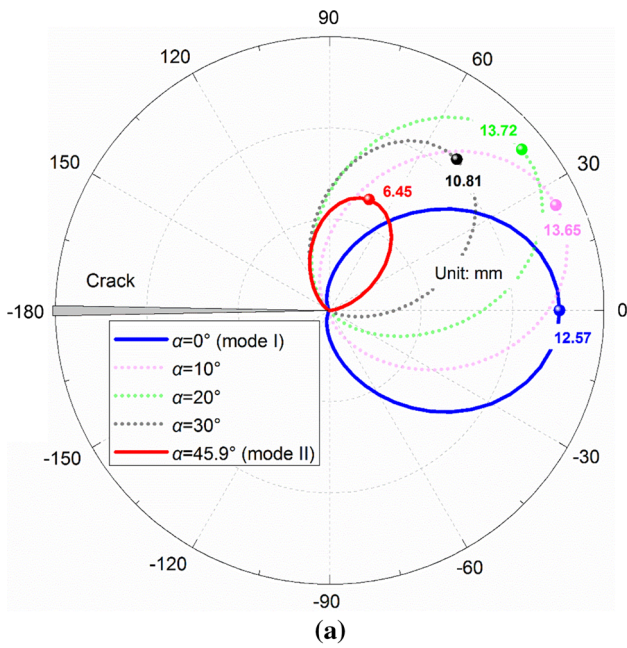


Fig. 14 Values of f_1 and f_2 determined based on the MTS and GMTS criteria, respectively: **a** f_1 , **b** f_2

stress is considered, r_0 gradually increases with increasing crack inclination angle; typically, the value of r_0 under mode II loading is nearly five times that under mode I loading. These facts clearly demonstrate that the T -stress has a significant influence on both the shape and size of the MCZ around a crack tip. To better understand the above issues, it is necessary to determine how the T -

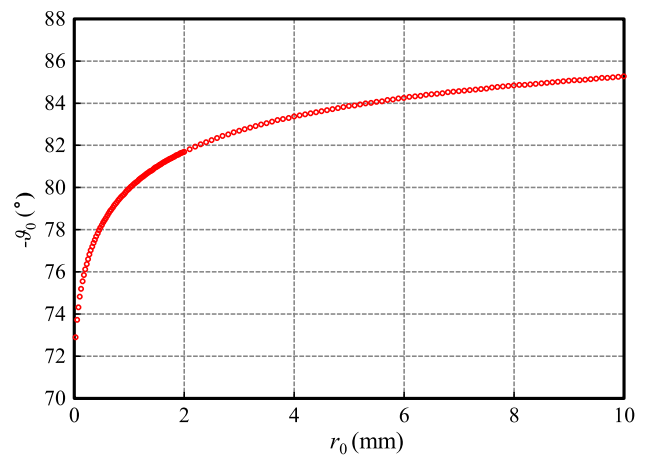


Fig. 15 Variations in the crack initiation angle ϑ_0 determined by the GMTS criterion with different r_0 for pure mode II loading

stress affects the MCZ. Table 2 shows that the T -stress is positive for loading conditions that are dominated by mode II and negative for loading conditions that are dominated by mode I. In the case of $\alpha = 0^\circ$ (under pure mode I loading), the crack will propagate along the original crack plane. Therefore, the maximum value of f_1 in Eq. (19) equals that of f_2 in Eq. (20), i.e., the T -stress has no influence on r_0 . Nevertheless, according to Eq. (20), a negative T -stress will decrease the radius of the MCZ if $\vartheta \neq 0^\circ$. For the case of $\alpha = 10^\circ$, the negative T -stress will also decrease the MCZ and result in the maximum value of f_1 being smaller than that of f_2 . In the case of $\alpha \geq 20^\circ$, the positive T -stress will clearly increase the dimensions of the MCZ, and the maximum value of f_1 will become larger than that of f_2 .

As mentioned above, in the GMTS criterion, r_0 is assumed to be a constant when predicting the crack initiation direction and the fracture strength. Taking the fracture problem under pure mode II loading as an example (see Fig. 15), the crack initiation angle ϑ_0 increases as r_0 increases. The crack initiation angle ϑ_0 determined by the GMTS criterion is particularly sensitive to r_0 when r_0 is a relatively small number. However, as indicated previously, r_0 is not a constant for all loading mixities regardless of whether the T -stress is considered. Therefore, there is a lack of both theoretical and experimental support for using the constant $r_0 = [1/(2\pi)](K_{Ic}/\sigma_t)^2$ in the GMTS criterion. Based on these results, r_0 must be chosen very carefully when applying the GMTS criterion; furthermore, the procedure for effectively and strictly determining the value of r_0 remains an important issue that should be further addressed.

8 Conclusions

In this paper, the test configuration of the NDB specimen was introduced for the fracture testing of rock materials under mixed-mode I/II loading, and a series of finite element analyses were performed to determine the crack tip parameters. Several NDB specimens made of sandstone were used to investigate the brittle fracture behavior of rocks under mixed-mode I/II loading, and the fracture surfaces were theoretically described using a statistical method. The obtained fracture strength results were then analyzed using several fracture mechanics criteria. Moreover, based on the concepts of the PS and MS, a detailed description of the MCZs that were formed in the sandstone samples under different mixed-mode loading conditions was presented based on the MTS and GMTS criteria. The following conclusions can be obtained from the presented theoretical and experimental data:

1. The NDB specimen configuration with a length-to-width ratio of 2.0 can enable the investigation of pure mode I loading, pure mode II loading, and any mixed-mode loading conditions in between. In addition, NDB specimens of any desired size can be easily obtained by simply cutting them from blocks of rock. Moreover, NDB specimens were successfully employed in this study to conduct fracture tests of a typical sandstone under several mixed-mode loading conditions.
2. A statistical analysis of the topographical characteristics of the fracture surfaces revealed that all the surfaces generated under different loading mixities were statistically identical; it was further demonstrated that only tensile mode failure occurred when the sandstone NDB specimens were subjected to mixed-mode I/II loading.
3. The mixed-mode fracture test results of sandstone using NDB specimens were consistent with the theoretical predictions obtained using the IR -criterion, using the empirical criterion with $\beta_I = 1.21$ and $\beta_{II} = 3.41$, and using the GMTS criterion with an FPZ size of 0.4 mm. However, the MTS and MSED criteria could not effectively estimate the mixed-mode fracture envelope of the sandstone.
4. For the tested sandstone NDB specimens, at inclination angles of $\alpha = 0^\circ$ (pure mode I), 10° , 20° , 30° , and 45.9° (pure mode II), the maximum values of f_1 were 12.57, 13.65, 13.72, 10.81, and 6.45 mm, respectively, and the maximum values of f_2 were 12.57, 13.39, 14.62, 16.56, and 62.83 mm. The negative (positive) T -stress could decrease (or increase) the size of the MCZ around the crack tip.
5. The results clearly show that r_0 is not a constant for all loading mixities regardless of whether the T -stress is

considered. Based on this result, it is suggested that the value of r_0 used in the GMTS criterion to predict the crack initiation direction and fracture strength should be chosen more carefully; furthermore, the procedure for effectively determining the value of r_0 for the GMTS criterion should be further investigated.

Acknowledgements The authors express their sincere gratitude to all the anonymous reviewers for their comments devoted to improving the quality of our paper. This paper was financially supported by the Major State Research Projects (2016YFC0600702) and Provincial Science and Technology Support Project of Sichuan Province (2015JY0280).

References

- Ai T, Zhang R, Zhou HW, Pei JL (2014) Box-counting methods to directly estimate the fractal dimension of a rock surface. *Appl Surf Sci* 314:610–621. doi:10.1016/j.apsusc.2014.06.152
- Aliha MRM, Ayatollahi MR (2011) Mixed mode I/II brittle fracture evaluation of marble using SCB specimen. *Procedia Eng* 10:311–318. doi:10.1016/j.proeng.2011.04.054
- Aliha MRM, Hosseinpour GR, Ayatollahi MR (2013) Application of cracked triangular specimen subjected to three-point bending for investigating fracture behavior of rock materials. *Rock Mech Rock Eng* 46:1023–1034. doi:10.1007/s00603-012-0325-z
- Atkinson C, Smelser RE, Sanchez J (1982) Combined mode fracture via the cracked Brazilian disk test. *Int J Fract* 18:279–291. doi:10.1007/BF00015688
- Awaji H, Sato S (1978) Combined mode fracture toughness measurement by the disk test. *J Eng Mater Technol* 100:175–182. doi:10.1115/1.3443468
- Ayatollahi MR, Aliha MRM (2007a) Fracture toughness study for a brittle rock subjected to mixed mode I/II loading. *Int J Rock Mech Min Sci* 44:617–624. doi:10.1016/j.ijrmmms.2006.10.001
- Ayatollahi MR, Aliha MRM (2007b) Wide range data for crack tip parameters in two disc-type specimens under mixed mode loading. *Comput Mater Sci* 38:660–670. doi:10.1016/j.comatsci.2006.04.008
- Ayatollahi MR, Aliha MRM, Hassani MM (2006) Mixed mode brittle fracture in PMMA—an experimental study using SCB specimens. *Mater Sci Eng, A* 417:348–356. doi:10.1016/j.msea.2005.11.002
- Babadagli T, Develi K (2003) Fractal characteristics of rocks fractured under tension. *Theor Appl Fract Mech* 39:73–88. doi:10.1016/S0167-8442(02)00139-8
- Backers T (2005) Fracture toughness determination and micromechanics of rock under mode I and mode II loading. Doctoral Thesis, University of Potsdam
- Backers T, Stephansson O (2012) ISRM suggested method for the determination of mode II fracture toughness. *Rock Mech Rock Eng* 45:1011–1022. doi:10.1007/s00603-012-0271-9
- Balzani C, Wagner W, Wilckens D, Degenhardt R, Büsing S, Reimerdes H-G (2012) Adhesive joints in composite laminates—a combined numerical/experimental estimate of critical energy release rates. *Int J Adhes Adhes* 32:23–38. doi:10.1016/j.ijadhadh.2011.09.002
- Carpinteri A, Cornetti P, Pugno N, Sapora A, Taylor D (2009) Generalized fracture toughness for specimens with re-entrant corners: experiments vs. theoretical predictions. *Struct Eng Mech* 32:609–620

- Chang S-H, Lee C-I, Jeon S (2002) Measurement of rock fracture toughness under modes I and II and mixed-mode conditions by using disc-type specimens. *Eng Geol* 66:79–97. doi:[10.1016/S0013-7952\(02\)00033-9](https://doi.org/10.1016/S0013-7952(02)00033-9)
- Chong KP, Kuruppu MD (1984) New specimen for fracture toughness determination for rock and other materials. *Int J Fract* 26:R59–R62. doi:[10.1007/BF01157555](https://doi.org/10.1007/BF01157555)
- Dai F, Chen R, Xia K (2010) A semi-circular bend technique for determining dynamic fracture toughness. *Exp Mech* 50:783–791. doi:[10.1007/s11340-009-9273-2](https://doi.org/10.1007/s11340-009-9273-2)
- Dai F, Wei MD, Xu NW, Ma Y, Yang DS (2014) Numerical assessment of the progressive rock fracture mechanism of cracked chevron notched Brazilian disc specimens. *Rock Mech Rock Eng* 48:463–479. doi:[10.1007/s00603-014-0587-8](https://doi.org/10.1007/s00603-014-0587-8)
- Erdogan F, Sih GC (1963) On the crack extension in plates under plane loading and transverse shear. *J Fluids Eng* 85:519–525. doi:[10.1115/1.3656897](https://doi.org/10.1115/1.3656897)
- Fowell RJ (1995) Suggested method for determining mode I fracture toughness using cracked chevron notched Brazilian disc (CCNBD) specimens. *Int J Rock Mech Min Sci* 32:57–64
- Funatsu T, Shimizu N, Kuruppu M, Matsui K (2014) Evaluation of mode I fracture toughness assisted by the numerical determination of K-resistance. *Rock Mech Rock Eng* 48:143–157. doi:[10.1007/s00603-014-0550-8](https://doi.org/10.1007/s00603-014-0550-8)
- Hasanpour R, Choupani N (2009) Rock fracture characterization using the modified Arcan test specimen. *Int J Rock Mech Min Sci* 46:346–354. doi:[10.1016/j.ijrmms.2008.07.004](https://doi.org/10.1016/j.ijrmms.2008.07.004)
- Hussain MA, Pu SL, Underwood J (1974) Strain energy release rate for a crack under combined mode I and mode II. *Fract Anal* 560:2–28. doi:[10.1520/STP33130S](https://doi.org/10.1520/STP33130S)
- Kfoury AP, Brown MW (1995) Fracture criterion for cracks under mixed-mode loading. *Fatigue Fract Eng Mater Struct* 18:959–969. doi:[10.1111/j.1460-2695.1995.tb00920.x](https://doi.org/10.1111/j.1460-2695.1995.tb00920.x)
- Khan SMA, Khraisheh MK (2000) Analysis of mixed mode crack initiation angles under various loading conditions. *Eng Fract Mech* 67:397–419. doi:[10.1016/S0013-7944\(00\)00068-0](https://doi.org/10.1016/S0013-7944(00)00068-0)
- Khan SMA, Khraisheh MK (2004) A new criterion for mixed mode fracture initiation based on the crack tip plastic core region. *Int J Plast* 20:55–84. doi:[10.1016/s0749-6419\(03\)00011-1](https://doi.org/10.1016/s0749-6419(03)00011-1)
- Kong XM, Schlüter N, Dahl W (1995) Effect of triaxial stress on mixed-mode fracture. *Eng Fract Mech* 52:379–388. doi:[10.1016/0013-7944\(94\)00228-A](https://doi.org/10.1016/0013-7944(94)00228-A)
- Kuruppu MD (1997) Fracture toughness measurement using chevron notched semi-circular bend specimen. *Int J Fract* 86:L33–L38
- Leguillon D (2002) Strength or toughness? A criterion for crack onset at a notch. *Eur J Mech A Solids* 21:61–72. doi:[10.1016/S0997-7538\(01\)01184-6](https://doi.org/10.1016/S0997-7538(01)01184-6)
- Lim IL, Johnston IW, Choi SK, Boland JN (1994) Fracture testing of a soft rock with semi-circular specimens under three-point bending. Part 2—mixed-mode. *Int J Rock Mech Min Sci* 31:199–212. doi:[10.1016/0148-9062\(94\)90464-2](https://doi.org/10.1016/0148-9062(94)90464-2)
- Luo L, Wang QZ (2009) Concurrent measurement of tensile strength and fracture toughness of quasi-brittle materials using U-notched beams: theoretical analysis. *Eng Mech* 26:244–250
- Mróz KP, Mróz Z (2010) On crack path evolution rules. *Eng Fract Mech* 77:1781–1807. doi:[10.1016/j.engfracmech.2010.03.038](https://doi.org/10.1016/j.engfracmech.2010.03.038)
- Nuismer RJ (1975) An energy release rate criterion for mixed mode fracture. *Int J Fract* 11:245–250. doi:[10.1007/BF00038891](https://doi.org/10.1007/BF00038891)
- Palaniswamy K, Knauss WG (1972) Propagation of a crack under general, in-plane tension. *Int J Fract* 8:114–117. doi:[10.1007/BF00185207](https://doi.org/10.1007/BF00185207)
- Rao Q, Sun Z, Stephansson O, Li C, Stillborg B (2003) Shear fracture (mode II) of brittle rock. *Int J Rock Mech Min Sci* 40:355–375. doi:[10.1016/S1365-1609\(03\)00003-0](https://doi.org/10.1016/S1365-1609(03)00003-0)
- Ren L, Zhu Z, Wang M, Zheng T, Ai T (2013a) Mixed-mode elastic-plastic fractures: improved R-criterion. *J Eng Mech* 140:04014033
- Ren L, Zhu Z, Yang Q, Ai T (2013b) Investigation on the applicability of several fracture criteria to the mixed mode brittle fractures. *Adv Mech Eng* 5:545108. doi:[10.1155/2013/545108](https://doi.org/10.1155/2013/545108)
- Ren L, Xie LZ, Li CB, Wang J (2014) Compressive fracture of brittle geomaterial: fractal features of compression-induced fracture surfaces and failure mechanism. *Adv Mater Sci Eng* 2014:814504. doi:[10.1155/2014/814504](https://doi.org/10.1155/2014/814504)
- Ren L, Xie LZ, Xie H, Ai T, He B (2016) Mixed-mode fracture behavior and related surface topography feature of a typical sandstone. *Rock Mech Rock Eng* 49:3137–3153. doi:[10.1007/s00603-016-0959-3](https://doi.org/10.1007/s00603-016-0959-3)
- Ritchie RO, Knott JF, Rice JR (1973) On the relationship between critical tensile stress and fracture toughness in mild steel. *J Mech Phys Solids* 21:395–410. doi:[10.1016/0022-5096\(73\)90008-2](https://doi.org/10.1016/0022-5096(73)90008-2)
- Schmidt RA (1980) Microcrack model and its significance to hydraulic fracturing and fracture toughness testing. In: 21st US symposium on rock mechanics (USRMS), American Rock Mechanics Association, Rolla, Missouri, pp 581–590
- Seweryn A (1998) A non-local stress and strain energy release rate mixed mode fracture initiation and propagation criteria. *Eng Fract Mech* 59:737–760. doi:[10.1016/S0013-7944\(97\)00175-6](https://doi.org/10.1016/S0013-7944(97)00175-6)
- Sheity DK, Rosenfield AR, Duckworth WH (1985) Fracture toughness of ceramics measured by a chevron-notch diametral-compression test. *J Am Ceram Soc* 68:C325–C327. doi:[10.1111/j.1151-2916.1985.tb10135.x](https://doi.org/10.1111/j.1151-2916.1985.tb10135.x)
- Sih GC (1974) Strain-energy-density factor applied to mixed mode crack problems. *Int J Fract* 10:305–321. doi:[10.1007/BF00035493](https://doi.org/10.1007/BF00035493)
- Smith DJ, Ayatollahi MR, Pavier MJ (2006) On the consequences of T-stress in elastic brittle fracture. *Proc Natl Acad Sci USA* 462:2415–2437. doi:[10.1098/rspa.2005.1639](https://doi.org/10.1098/rspa.2005.1639)
- Susmel L, Taylor D (2008) The theory of critical distances to predict static strength of notched brittle components subjected to mixed-mode loading. *Eng Fract Mech* 75:534–550. doi:[10.1016/j.engfracmech.2007.03.035](https://doi.org/10.1016/j.engfracmech.2007.03.035)
- Swartz SE, Taha NM (1990) Mixed mode crack propagation and fracture in concrete. *Eng Fract Mech* 35:137–144. doi:[10.1016/0013-7944\(90\)90191-I](https://doi.org/10.1016/0013-7944(90)90191-I)
- Theocaris PS, Andrianopoulos NP (1983) Failure theories for glassy polymers: the T-criterion for various yield loci. *Pure Appl Chem* 55:845–852. doi:[10.1351/pac198355050845](https://doi.org/10.1351/pac198355050845)
- Wang QZ, Feng F, Ni M, Gou XP (2011) Measurement of mode I and mode II rock dynamic fracture toughness with cracked straight through flattened Brazilian disc impacted by split Hopkinson pressure bar. *Eng Fract Mech* 78:2455–2469. doi:[10.1016/j.engfracmech.2011.06.004](https://doi.org/10.1016/j.engfracmech.2011.06.004)
- Wang J, Ren L, Xie LZ, Xie HP, Ai T (2016) Maximum mean principal stress criterion for three-dimensional brittle fracture. *Int J Solids Struct* 102–103:142–154. doi:[10.1016/j.ijsolstr.2016.10.009](https://doi.org/10.1016/j.ijsolstr.2016.10.009)
- Whitcomb JD (1986) Parametric analytical study of instability-related delamination growth. *Compos Sci Technol* 25:19–48. doi:[10.1016/0266-3538\(86\)90019-9](https://doi.org/10.1016/0266-3538(86)90019-9)
- Williams ML (1957) On the stress distribution at the base of a stationary crack. *J Appl Mech* 24:109–114
- Wu C-H (1978) Fracture under combined loads by maximum-energy-release-rate criterion. *J Appl Mech* 45:553–558. doi:[10.1115/1.3424360](https://doi.org/10.1115/1.3424360)
- Yehia NAB, Shephard MS (1987) The NT-criterion for predicting crack growth increments. *Eng Fract Mech* 26:371–382. doi:[10.1016/0013-7944\(87\)90019-1](https://doi.org/10.1016/0013-7944(87)90019-1)
- Zhang X, Jeffrey RG, Bungler AP, Thiercelin M (2011) Initiation and growth of a hydraulic fracture from a circular wellbore. *Int J Rock Mech Min Sci* 48:984–995. doi:[10.1016/j.ijrmms.2011.06.005](https://doi.org/10.1016/j.ijrmms.2011.06.005)

- Zhang R, Ai T, Li H, Zhang Z, Liu J (2013) 3D reconstruction method and connectivity rules of fracture networks generated under different mining layouts. *Int J Rock Mech Min Sci* 23:863–871. doi:[10.1016/j.ijmst.2013.10.013](https://doi.org/10.1016/j.ijmst.2013.10.013)
- Zhang R, Ai T, Zhou HW, Ju Y, Zhang ZT (2015) Fractal and volume characteristics of 3D mining-induced fractures under typical mining layouts. *Environ Earth Sci* 73:6069–6080. doi:[10.1007/s12665-015-4376-9](https://doi.org/10.1007/s12665-015-4376-9)
- Zhao Y (1990) Elliptic rule criterion for mixed mode crack propagation. *Eng Fract Mech* 37:283–292. doi:[10.1016/0013-7944\(90\)90041-E](https://doi.org/10.1016/0013-7944(90)90041-E)
- Zhou HW, Xie H (2003) Direct estimation of the fractal dimensions of a fracture surface of rock. *Surf Rev Lett* 10:751–762. doi:[10.1142/S0218625X03005591](https://doi.org/10.1142/S0218625X03005591)